Journal of Physics: Conference Series **490** (2014) 012051 doi:10.1088/1742-6596/490/1/012051

Structure of genuine and conjugate Fermi holes and the first Hund rule in He-like systems

Tokuei Sako

Laboratory of Physics, College of Science and Technology, Nihon University, 7-24-1 Narashinodai, Funabashi, 274-8501 Chiba, Japan

E-mail: sako@phys.ge.cst.nihon-u.ac.jp

Abstract. The singly-excited states of He and He-like atomic ions in the manifold of the $n = 3$ principal shell have been studied replying on the full configuration interaction wave function focusing on the origin of the first Hund rule. The probability density distributions of the singlet-triplet pairs of states for the three orbital configurations of $(1s)(3s)$, $(1s)(3p)$, and $(1s)(3d)$ have been examined in detail in the internal space (r_1, r_2, ϕ_-). The structure of the genuine and *conjugate Fermi holes* for the $(1s)(3s)$ and $(1s)(3p)$ configurations has shown similar characteristics to those for the respective $(1s)(2s)$ and $(1s)(2p)$ configurations examined in an earlier study. A significantly smaller size of the genuine and conjugate Fermi holes for the $(1s)(3d)$ singlet-triplet pair of states rationalizes the much smaller singlet-triplet energy gap of this pair than those for the $(1s)(3s)$ and $(1s)(3p)$ pairs of states.

1. Introduction

Hund's rule [1, 2, 3] is one of the most fundamental rules in atomic physics, that predicts the ordering of energy levels possessing the same orbital configuration yet different spin and orbital angular momentum quantum numbers. The first Hund rule, concerning the spin multiplicity, is particularly universally valid not only for atomic systems but for molecules [4] and artificial atoms [5, 6]. Despite the past long standing debates [7, 8, 9, 10, 11] focusing mainly on the relative importance of the energy components, such as the electron-nuclear attraction energy vs. the electron-electron repulsion energy, the search for its origin persists primary due to a lack of precise knowledge of the electronic structure of atoms for different spin states.

We have recently shown that for the singly-excited S and P states arising from the $(1s)(2s)$ and $(1s)(2p)$ configurations in the He and He-like atomic ions the origin of Hund's rule can be rationalized on the basis of the structure of the so-called genuine and *conjugate Fermi holes* [12, 13]. In the present study we have extended our analysis for different angular momentum states of singly-excited manifold of He-like systems and thus presented a unified understanding for the origin of this historical rule.

2. Theoretical model and computational methodology

In our previous study the so-called two-dimensional Helium model has been used in which the spatial degrees of freedom of the two electrons are confined to a two-dimensional xy plane with the nucleus place at the origin. The Hamiltonian of this two-dimensional He-like systems reads

in atomic units as

$$\mathcal{H}_Z = -\frac{1}{2}\sum_{i=1}^{2}\nabla_i^2 - \sum_{i=1}^{2}\frac{Z_{\rm n}}{|\vec{r}_i|} + \frac{1}{|\vec{r}_1-\vec{r}_2|}, \tag{1}$$

where $\vec{r}_i = (x_i, y_i)$ $[= r_i(\cos\phi_i, \sin\phi_i)]$ for $i = 1, 2$, while $Z_{\rm n}$ represents the nuclear charge. Our previous study showed that this *two-dimensional helium model* reproduces all the characteristic features of the energy spectrum of the real 3D helium atom [12]. By reducing the dimensionality and thus the number of the degrees of freedom the *internal* part of the wave functions can be easily visualised. This allows an unambiguous manifestation of the origin of the Hund rule. By introducing a scaling for the coordinates with the nuclear charge $Z_{\rm n}$ such as $\vec{s}_i \equiv Z_{\rm n}\vec{r}_i$ the Hamiltonian becomes

$$\mathcal{H}_Z/Z_{\rm n}^2 = -\frac{1}{2}\sum_{i=1}^{2}\nabla_{s,i}^2 - \sum_{i=1}^{2}\frac{1}{|\vec{s}_i|} + \frac{1}{Z_{\rm n}}\frac{1}{|\vec{s}_1-\vec{s}_2|}. \tag{2}$$

This scaled Hamiltonian indicates that the one-electron part, namely, the kinetic energy plus the electron-nuclear attraction energy, is independent of $Z_{\rm n}$ while not the electron-electron repulsion energy. The factor $\frac{1}{Z_{\rm n}}$ in front of the last term in the right-hand side of Eq. (2) guarantees that the electron-electron interaction becomes smaller relative to the one-electron energy as $Z_{\rm n}$ decreases. Two-dimensional Cartesian Gaussian-type functions of the form

$$\chi^{\vec{a},\zeta}(\vec{r}) = x^{a_x}y^{a_y}\exp[-\zeta(x^2+y^2)] \tag{3}$$

have been used to expand the one-electron orbitals for the scaled Hamiltonian (2). A detailed description of the basis set may be found elsewhere [13].

The energy and wave function of the Hamiltonian (2) has been obtained by diagonalising the full configuration interaction (full CI) matrix. The *internal space* of the two-electron He-like systems may be defined by the three variables (r_1, r_2, ϕ_-) [12, 13] where $r_i \equiv |\vec{r}_i|$ for i=1,2 and $\phi_- \equiv (\phi_1 - \phi_2)/2$. The angle variable complementary to ϕ_- defined by $\phi_+ \equiv (\phi_1 + \phi_2)/2$ is associated with the total angular momentum L. The probability density distribution in the internal space $\rho(r_1, r_2, \phi_-)$ is thus obtained from the full CI wave function $\Psi(r_1, \phi_1, r_2, \phi_2)$ by integrating the square norm of Ψ with the ϕ_+ variable. The detail of the procedure may be found in an earlier paper [12].

3. Fermi and conjugate Fermi holes

The genuine and conjugate Fermi holes are defined by the difference between the probability density distributions of the singlet state and of the corresponding triplet state comprising the Hund's pair of states in the limit of $Z_{\rm n} = \infty$ [12, 13]. By considering this large limit of the nuclear charge they are uniquely defined by the pair of zeroth-order one-electron orbitals that are the eigenfunctions of the one-electron part of the Hamiltonian (2). It is noted that in this large $Z_{\rm n}$ limit the singlet and triplet wave functions give exactly the same electron density distributions. Therefore, their difference in the probability density distributions in the internal space is caused solely by the difference in the symmetry properties of their spatial wave functions with respect to exchanging the spatial coordinates of electron 1 and 2, i.e., symmetric and antisymmetric for the singlet and triplet wave functions, respectively. The difference in the topological structure between the genuine and conjugate Fermi holes allows us an insightful visualization of the variation of the singlet and triplet states, and thus the origin of the lower energy of the triplet state than the counter part singlet state.

The genuine and Fermi holes for the $(1s)(3s)$ and $(1s)(3p)$ configurations have been plotted in Figs. 1 (a) and (b), respectively. The blue and red surfaces displayed in this figure represent, respectively, the regions where the probability density of the singlet state is larger than that of

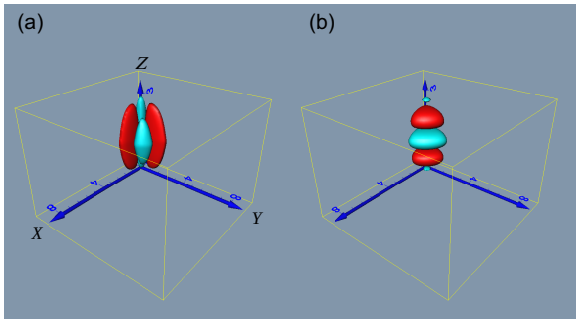

Figure 1. The genuine and conjugate Fermi holes in the internal space (r_1, r_2, ϕ_-) for the $(1s)(3s)$ and $(1s)(3p)$ singlet-triplet pairs of states [(a) and (b), respectively] of He-like systems. The X, Y, and Z axes represent r_1, r_2, and ϕ_-, respectively. The probability density at the displayed surface is 5.0×10^{-4}.

the triplet state, and vice versa. The density at the surfaces is 5.0×10^{-4}. Inside the blue surfaces the probability density of the triplet state is much smaller than that of the corresponding singlet state. Therefore, these regions represent the so-called standard Fermi holes. On the other hand, inside the red surfaces the probability density of the singlet state in turn is much smaller than the triplet state, that have been defined and called as the *conjugate Fermi holes* in earlier studies [12, 13]. The existence of these conjugate Fermi holes as well as the genuine ones can be rationalized as follows.

The spatial part of the wave functions of the singlet-triplet pair of states for the $(1s)(nl)$ configuration in the limit of $Z_{\rm n}\rightarrow\infty$ can be described as

$$\Psi^{\pm}_{nl} = \frac{1}{\sqrt{2}}[\psi_{1s}(\vec{r}_1)\psi_{nl}(\vec{r}_2) \pm \psi_{nl}(\vec{r}_1)\psi_{1s}(\vec{r}_2)], \tag{4}$$

where the symmetric and antisymmetric wave functions, Ψ^{+}_{nl} and Ψ^{-}_{nl}, represent, respectively, the singlet and triplet states. By choosing $\vec{r}_1 = \vec{r}_2$ for the triplet Ψ^{-}_{nl} wave function, the first and second terms in the bracket of the right hand side of Eq. (4) cancel with each other. This results in the well-known Fermi holes as indicated by the blue regions in Fig. 1. In the case of the singlet Ψ^{+}_{nl} wave function this cancellation doesn't occur for $\vec{r}_1 = \vec{r}_2$ because of its symmetric nature. However, another type of 'cancellation' can occur for the singlet wave function: As is well known the ψ_{nl} orbital has at least one node [radial node(s) for $n > 2$ and/or angular node(s) for $l > 0$] where the amplitude becomes zero. Therefore, this orbital changes its sign when the argument crosses the node point. By arbitrary choosing two points, designated by $\vec{r}_{\rm A}$ and $\vec{r}_{\rm B}$, so that they cross this node point and putting them into the singlet wave function as $\Psi^{+}_{nl}(\vec{r}_{\rm A}, \vec{r}_{\rm B})$, the first and second terms in the bracket of the right hand side of Eq. (4) cancel with each other since $\psi_{nl}(\vec{r}_{\rm A})$ and $\psi_{nl}(\vec{r}_{\rm B})$ have different signs. In the case of the triplet Ψ^{+}_{nl} wave function this cancellation doesn't occur since the minus sign in front of the second term compensates the change of the sign in the ψ_{nl} orbital. Therefore, in the vicinity of $(\vec{r}_{\rm A}, \vec{r}_{\rm B})$ the triplet wave functions should have much larger probability density than the singlet wave functions. This guarantees the existence of the conjugate Fermi holes as indicated by the red surfaces in Fig. 1.

The genuine and conjugate Fermi holes displayed in Fig. 1 look quite similar to those for the $(1s)(2s)$ and $(1s)(2p)$ configurations examined in detail in earlier studies [12, 13]. The main difference between the two configurations, $(1s)(2s)$ and $(1s)(3s)$, and between $(1s)(2p)$ and $(1s)(3p)$ is that the outer orbitals, $(3s)$ and $(3p)$, in the higher principle shell of $n = 3$ have an additional radial node than the corresponding $(2s)$ and $(2p)$ orbitals in the lower shell. The reason for the topological similarity in their genuine and conjugate holes in spite of the existence of this additional radial node is that genuine and conjugate Fermi holes exist in the regions where the two orbitals, ψ_{1s} and ψ_{nl}, constituting the wave function of Eq. (4) spatially overlap with each other. Therefore, since the node point of this additional node in the higher n shell is far away from the small r region where the maximum density of the tight $(1s)$ orbital resides, it does hardly contribute to the formation of genuine and conjugate Fermi holes. Thanks

to the similarity in the structure of the genuine and conjugate Fermi holes between the $(1s)(2s)$ and $(1s)(3s)$ configurations and between $(1s)(2p)$ and $(1s)(3p)$, the mechanism of the origin of the first Hund rule operating in the $(1s)(2s)$ and $(1s)(2p)$ configurations described in detail in earlier papers [12, 13] can be applied to the present $(1s)(3s)$ and $(1s)(3p)$ cases.

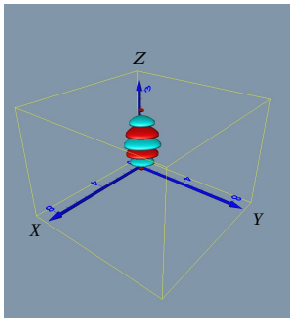

Figure 2. The genuine and conjugate Fermi holes in the internal space (r_1, r_2, ϕ_-) for the $(1s)(3d)$ singlet-triplet pair of states of He-like systems. The probability density at the displayed surface is 5.0×10^{-5}. See the caption to Fig. 1 for other remarks.

The genuine and conjugate Fermi holes for the $(1s)(3d)$ configuration have been displayed in Fig. 2. It is noted that the density at the displayed surface in this figure is 5.0×10^{-5}, 10 times smaller than that for Fig. 1. Therefore, the integrated probability density in the genuine and conjugate holes for this $(1s)(3d)$ configuration is much smaller than those for the $(1s)(3s)$ and $(1s)(3p)$ configurations. Since the density in the genuine and conjugate holes determines the difference between the singlet and triplet states, the significantly smaller density of the $(1s)(3d)$ configurations indicates a much smaller energy difference than the cases for the $(1s)(3s)$ and $(1s)(3p)$ configurations. This is consistent with the experimental observation that the singlet-triplet energy gap for this $(1s)(3d)$ pair of states is significantly smaller than those for the $(1s)(3s)$ and $(1s)(3p)$ pairs of states.

4. Acknowledgments

The present study has been supported in parts by Grants-in-Aid for Scientific Research (No 23550025) from the Ministry of Education, Culture, Sports, Science and Technology (MEXT) and by Nihon University Strategic Projects for Academic Research. The author would like to thank Prof. Geerd H. F. Diercksen and Prof. Josef Paldus for helpful discussion.

References

[1] Hund F 1925 *Z. Phys.* **33** 345
[2] Hund F 1925 *Z. Phys.* **34** 296
[3] Hund F 1927 *Linienspektren und periodisches System der Elemente* (Springer, Berlin) pp. 98, 124
[4] Colpa J P and Brown R E 1973 *Mol. Phys.* **26** 1453
[5] Sajeev Y, Sindelka M, and Moiseyev N 2008 *J. Chem. Phys.* **128** 061101
[6] Sako T, Paldus J, and Diercksen G H F 2010 *Phys. Rev. A* **81** 022501
[7] Davidson E R 1964 *J. Chem. Phys.* **41** 656-658
[8] Davidson E R 1965 *J. Chem. Phys.* **42** 4199-4200
[9] Katriel J and Pauncz R 1977 *Adv. Quantum Chem.* **10** 143-185
[10] Boyd R J 1984 *Nature* **310** 480-481
[11] Oyamada T, Hongo K, Kawazoe Y, and Yasuhara H 2010 *J. Chem. Phys.* **133** 164113
[12] Sako T, Paldus J, Ichimura A, and Diercksen G H F 2011 *Phys. Rev. A* **83** 032511
[13] Sako T, Paldus J, Ichimura A, and Diercksen G H F 2012 *J. Phys. B* **45** 235001